UC San Diego
UC San Diego Previously Published Works

Title

Distributed Strain Sensing Using Electrical Time Domain Reflectometry With Nanocomposites

Permalink

Journal

ISSN

Authors

Lee, Bo Mi
Loh, Kenneth J
di Scalea, Francesco Lanza

Publication Date

2018

DOI

Peer reviewed

Distributed Strain Sensing using Electrical Time Domain Reflectometry with Nanocomposites

Bo Mi Lee, Kenneth J. Loh, Member, *IEEE*, and Francesco Lanza di Scalea, Senior Member, *IEEE*

Abstract—The objective of this study is to validate distributed strain sensing using Electrical Time Domain Reflectometry (ETDR) with multi-walled carbon nanotube (MWCNT)-based thin film sensing elements. The proposed ETDR sensor composed of two types of transmission lines: parallel-wire-type transmission line and parallel-plate-type transmission line (*i.e.*, with MWCNT-based sensing elements). The hypothesis was that greater strain-induced impedance changes of the nanocomposite would enhance ETDR sensing performance. In this study, four different types of ETDR sensing elements were subjected to one-cycle uniaxial tensile strains to validate strain sensing. Three sensing elements were then integrated in an ETDR setup, and strain patterns were applied for validating their distributed strain sensing behavior.

Index Terms—Carbon nanotubes, electrical time domain reflectometry, strain sensing, thin film, transmission line.

I. INTRODUCTION

THE performance of aerospace, civil, marine, and mechanical structural systems can degrade due to damage and deterioration, particularly because of fatigue, impact, excessive loading, and harsh environmental conditions. If damage remains undetected, it can accumulate and propagate to cause component or even system failure. Therefore, structural health monitoring (SHM) aims to monitor target structures over time (either periodically or continuously), detect anomalies, and extract damage-sensitive features from measurements [1]. To date, the most widely used means of monitoring damage is by visual inspection, but it is time-consuming, expensive, and challenging, especially when structures are large, have complex geometries, and damage can occur at different locations.

Among the various parameters of interest (*i.e.*, displacement, crack opening, temperature, and humidity), knowledge of stress and strain is critical, since the failure criterion is often defined according to the material's yield point or ultimate strength. Without a practical method to directly measure stress, stress can be estimated from strain along with *a priori* information about material properties and behavior. Conventional means of measuring strain is by using metal foil strain gages. Although they are low-cost and fairly accurate, their main limitation is that they are discrete transducers that can only acquire strain at their instrumented location. For practical applications, a dense array of strain gages is required, but a number of cables that

connect gages to the data acquisition system can make implementation challenging and expensive [2]. To circumvent this drawback, fiber Bragg grating (FBG) optical sensors offer the unique capability of measuring strains, although they are still limited measurements at discrete locations along the optical fiber. While they are immune to electromagnetic (EM) interference and are highly sensitive to strains [3], their complex and expensive data acquisition system, as well as their high manufacturing and installation costs, can limit their use cases. More importantly, FBG sensors do not provide truly distributed sensing, since they can only monitor structural strains at a finite number of locations.

In order to overcome the discrete sensing limitation of traditional FBGs, the fiber optic sensing community has developed sensors based on Rayleigh or Brillouin scattering principles. These sensors provide distributed sensing of strain, with spatial resolutions on the order of a few centimeters, by monitoring changes in the light scattering properties caused by strain [4, 5]. More specifically, Rayleigh scattering is caused by non-propagating elastic density fluctuations, whereas Brillouin scattering is based on the inelastic interaction of sound waves traveling in opposite directions. Distributed sensing in Rayleigh and Brillouin scattering fiber optic sensors are achieved by various versions of Optical Time Domain Reflectometry (OTDR) [6, 7]. This implementation of OTDR requires a very large frequency bandwidth of the probing light in order to achieve small spatial resolution on the order of millimeters. The need for a tunable laser light source complicates the system and poses additional limits to the achievable scan rate, which, in turn, limits the range of dynamic strain measurements.

In contrast, Electrical Time Domain Reflectometry (ETDR) is used in the power and communication industries to locate faults at any point along a transmission line. ETDR entails propagating an EM pulse in the transmission line and then observing characteristics of the reflected pulse. The duration, shape, and magnitude of the reflected waveform contain rich information about impedance variations in the transmission system.

Early studies in geotechnical engineering introduced ETDR for rock deformation detection [8] and soil water content measurements [9]. For SHM applications, Liu *et al.* [10] suggested a twin-conductor transmission line that consisted of a bridge cable and a sensor wire for detecting steel cable
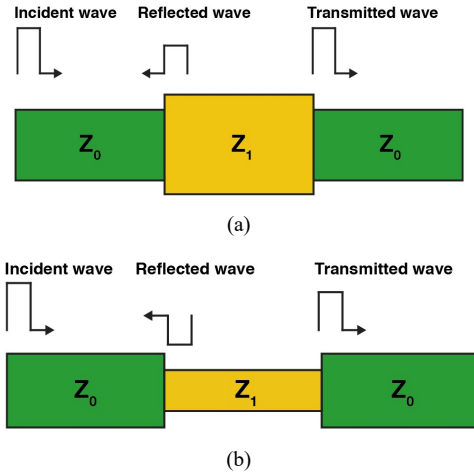
B. M. Lee, K. J. Loh, and F. Lanza di Scalia are with University of California-San Diego, 9500 Gilman Drive, MC 0085, La Jolla, CA 92093-0085, U.S.A. (corresponding author e-mail: kenloh@ucsd.edu).

Fig. 1. An impedance mismatch in a transmission line creates a reflected wave (a) if $Z_1 > Z_0$ or (b) $Z_1 < Z_0$.

corrosion. Corrosion was simulated by cutting several strands of the 0.95-m-long steel cable, and simulated damage locations were successfully determined from ETDR measurements. Lin *et al.* [11] replaced the dielectric part of a coaxial cable with rubber and compared its strain sensing response with that of an RG-174 cable that uses either polyethylene or Teflon for its dielectric. ETDR results showed that the proposed coaxial cable sensor was more sensitive to strains, which was enabled by the greater compliance of rubber. Unlike fiber optic sensors, its simple system architecture without the need of a laser light source, as well as low manufacturing and installation costs, would make ETDR implementation easier.

The main objective of this study is to leverage the principles of ETDR for developing and validating a distributed strain sensing system for SHM. Strain sensing was enabled by replacing portions of the transmission line with piezoresistive nanocomposite sensing elements. In particular, multi-walled carbon nanotubes (MWCNT) were used to modify the conductor and dielectric portions of the sensing element, which resulted in four unique sample sets. The ETDR sensing properties of these different sample sets were characterized and compared systematically. Simultaneously, strain sensing along different points in a transmission line was also validated.

This paper begins with a brief background discussion of ETDR. This is followed by describing how the MWCNT-based sensing elements were fabricated, as well as the different strain sensing test protocols employed in this study. Next, the ETDR strain sensing results of the different sample sets, as well as sensing strain at multiple points in a single transmission line, are discussed. The paper concludes with a brief summary of the main findings and contributions of this research.

II. DISTRIBUTED SENSING USING ETDR

A. ETDR background

ETDR is an electrical measurement technique that propagates an EM wave in a transmission line and examines the reflected wave in the line. A transmission line is an electrical conductor designed to carry alternating current (AC), and its length is longer than 10% of an EM wavelength [12]. If there is any discontinuity in the characteristic impedance along the transmission line due to damage, that portion induces a reflected wave due to impedance mismatch. The reflection is generally quantified by a reflection coefficient (Γ) defined by the amplitude of the reflected voltage wave (V^-) normalized by the amplitude of the incident voltage wave (V^+) [12]:

$$\Gamma = \frac{V^-}{V^+} = \frac{Z_1 - Z_0}{Z_0 + Z_1} \tag{1}$$

where Z_0 and Z_1 are the characteristic impedances before and after the discontinuity, respectively (Fig. 1). When the transmission line is intact, where $Z = Z_0 = Z_1$, there is no reflected wave, and the EM wave will continue to propagate in the line. On the other hand, when an impedance discontinuity ($Z_0 \neq Z_1$) exists, a wave that carries the information about the discontinuity will be reflected (Fig. 1).

Here, two different scenarios are illustrated. First, when $Z_1 > Z_0$, it creates a positive reflection ($\Gamma > 0$) (Fig. 1(a)). Second, when $Z_1 < Z_0$, negative reflection is induced ($\Gamma < 0$) (Fig. 1(b)). With the known propagation velocity of the incident wave (v) and the measured time difference between the incident and reflected waves (Δt), the location of impedance discontinuity (l) can be determined:

$$l = \frac{v \Delta t}{2} \tag{2}$$

B. ETDR sensors

The distributed electrical characteristics of a transmission line are described by its series resistance (R), series inductance (L), shunt conductance (G), and shunt capacitance (C) [12]. An equivalent electrical circuit of a typical transmission line is shown in Fig. 2(a). Three approaches have been used to design an ETDR sensor for SHM, namely by: i) employing a conventional transmission line; ii) adjusting the geometry of the transmission line; and iii) incorporating the target structure as part of the transmission line.

First, Lin *et al.* [13] used a commercial coaxial cable transmission line to detect cracks in a reinforced concrete beam. However, conventional transmission lines are intended to transmit EM signals such that their geometry and dielectric materials are designed to prevent reflections during varying environmental conditions [14]. Therefore, if a typical
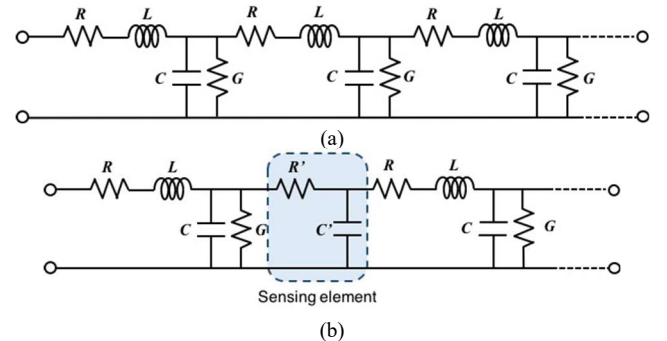

Fig. 2. (a) An equivalent circuit of a transmission line can be described by R, L, C, and G, and (b) a modified transmission line with an MWCNT-based sensing element can be modeled using R' and C'.

transmission line is used for measuring structural response, impedance changes are barely induced, and its sensitivity might not be enough for practical monitoring applications. Second, to improve sensitivity, Chen *et al.* [15] modified the geometry of the outer part of a coaxial cable with spiral wrapping so that the gap between adjacent spirals separate easily when subjected to mechanical loading. Finally, another approach is to use the monitored structure as part of the ETDR system [16, 17]. Todoroki [16] used carbon fiber-reinforced polymer (CFRP) as the conducting part of a transmission line to monitor bearing failure. The transmission line had a sandwiched structure of copper tape (*i.e.*, signal conducting layer), glass fiber-reinforced polymer (GFRP) (*i.e.*, dielectric layer), and CFRP composite (*i.e.*, electrical ground layer). A 6 mm-diameter fastener hole was created in a 200 mm × 1,850 mm specimen, and several impact loadings (10-30 J) were applied to the fastener by dropping weights. Impact damage was captured by ETDR when the energy of impact load was larger than 20 J. Pandey *et al.* [17] used a conductive layer with GFRP-based composites as the dielectric part and two copper plates as conductors. The copper plates were connected to a coaxial cable for EM signal propagation. The specimen was subjected to cyclic loading-unloading, and the results showed that the ETDR response followed the applied strains.

This study proposes a unique approach to design distributed ETDR strain sensors by integrating piezoresistive MWCNT-based sensing elements at different locations along the transmission line. In this case, the transmission line was a parallel wire (*i.e.*, speaker wire), which can be modeled by Fig. 2(a) with four electrical components (R, L, C, and G). The MWCNT-based sensing element was a parallel-plate capacitor with two conductive layers (*i.e.*, MWCNT thin films or copper tapes) separated by a dielectric layer of MWCNT-epoxy or pristine epoxy, which can be modeled as an *RC* element [18, 19] (Fig. 2(b)). The rationale for using the MWCNT-based elements was because of their intrinsic piezoresistivity, which can be tuned and controlled during nanocomposite fabrication for improving strain sensitivity. In addition, a parallel-plate-type transmission line sensing element was used, since uniform penetration of EM fields can enhance sensitivity [17].

III. EXPERIMENTAL DETAILS

A. Materials

MWCNTs were purchased from NanoIntegris. UV-curable epoxy (OG198-54) was acquired from EPO-TEK®. Pluronic F-127 (Pluronic) (M_W = 12,600) was from Sigma-Aldrich. Dragon Skin® FX-Pro (Dragon Skin) was acquired from Smooth-On. Hydrophilic polytetrafluoroethylene (PTFE) membrane filters (diameter: 47 mm and pore size: 0.2 μm) were purchased from EMD Millipore.

B. Nanocomposite sensor background

Recently, a new SHM approach employing sensors functionalized by nanomaterials (*e.g.*, carbon black [20], graphene [21, 22], carbon nanotubes [23, 24], nanoparticles [25,

26], and their hybrid [27]) has been introduced. The potential is that desired sensing properties can be realized by judiciously choosing nanomaterials [28], changing nanocomposite constituents [29], and controlling nanostructures [30]. In particular, carbon nanotubes (CNT) have received enormous attention due to their outstanding electromechanical properties and intrinsic piezoresistivity. For example, CNTs have been dispersed in polymers to realize nanocomposite sensors whose electrical properties change when subjected to strains [31-34].

C. Nanocomposite sensing element fabrication

The ETDR parallel-plate nanocomposite sensing element fabrication started with the preparation of its conducting part, which was the MWCNT-Pluronic thin film. Here, 1 mg/mL MWCNTs were dispersed in 0.5 wt% Pluronic solution. Dispersion was achieved by subjecting the mixture to 60 min of high-energy tip sonication. Second, two types of MWCNT-Pluronic thin films were assembled. MWCNT thin film #1 was fabricated by vacuum filtering the MWCNT-Pluronic dispersion using a PTFE membrane. Fabrication of MWCNT thin film #2 followed the same procedure, except that a 30 kHz AC voltage of 2.8 kV$_{\text{p-p}}$ was applied to the solution for 10 min, immediately prior to it being vacuum filtered; the resulting electric field, E, was 87.5 V$_{\text{p-p}}$/mm. It should be noted that E was applied to the solution using two parallel-plate electrodes mounted on opposite sides of the 3D-printed chamber directly above the filtering membrane and setup. Upon filtration, the thin films were air-dried for 12 h. The film was cut to form rectangular specimens (3 mm × 22 mm or 3 mm × 11mm). Specifically, MWCNT thin film #2 was cut such that the electric field direction is parallel to the longer side of the thin films. Scanning electron microscope (SEM) images of MWCNT thin films show that, unlike MWCNT thin film #1 that had a randomly dispersed network (Fig. 3(a)), MWCNT thin film #2 shows nanotube alignment in the direction of the applied field due to dielectrophoresis [35] (Fig. 3(b)).

The dielectric portion of the ETDR sensors was based on two different thick films (*i.e.*, epoxy and 1 wt% MWCNT-epoxy) to study how their dielectric properties affected strain sensing. Preparation of the dielectric begun by dispersing MWCNTs in epoxy via high-speed shear-mixing for 2 min at 3,500 rpm and then high-energy tip sonication for 2 min. This was repeated five times for achieving uniform dispersion. The viscous mix was then cast in dog-bone shaped Dragon Skin molds. Curing was performed using an ultraviolet (UV) lamp (Uvitron Porta-ray 400R) for 10 min, followed by curing in a Yamato ADP-300C oven for 12 h at 70 °C. Preparation of the pristine epoxy followed the same curing process. The thickness of the final dog-bone shaped epoxy thick films was ~ 1.15 mm (Fig. 4(a)).

The parallel-plate sensing element was then formed by attaching the conductive portion (*e.g.*, MWCNT-Pluronic thin film) to both the top and bottom of the dielectric (*e.g.*, MWCNT-epoxy). Electrodes were created at opposite ends of the thin films using copper tape (3 mm × 10 mm) and then drying colloidal silver paste (Ted Pella) at their interface to minimize contact impedance. These electrodes were then connected to speaker wires by soldering (Fig. 4(b)). Finally, a
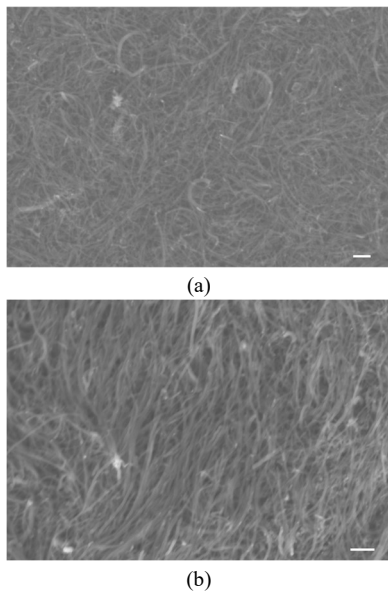
(a)

(b)

Fig. 3. SEM images of (a) the randomly dispersed MWCNT-Pluronic thin film (MWCNT thin film #1) and (b) the aligned MWCNT-Pluronic thin film (MWCNT thin film #2) are shown. The scale bar represents 200 nm.

BNC connector was soldered to one end of the wire (Fig. 4(c)) for ETDR interrogation and measurement purposes.

D. ETDR sensor sample sets

In this study, five unique ETDR sample sets were prepared. Four of them (*i.e.*, Sensors #1 to #4) were composed of two uniform lengths of parallel wires (l = 7.62 m) connected to opposite ends of the sensing element (Fig. 5(a)). These sensors were used to study how their R and C properties affected strain sensing capability (Fig. 2(b)). Sensor #1 (Fig. 6(a)) was the control sample set and consisted of two parallel copper tape strips (3 mm × 38 mm) attached to a dog-bone-shaped epoxy dielectric. Sensor #2 (Fig. 6(b)) employed MWCNT thin film #1 for the conductor, separated by pristine epoxy. Sensor #3 (Fig. 6(c)) also used MWCNT thin film #1 for the conductor but was separated by the MWCNT-epoxy thick film as the dielectric. Sensor #4 (Fig. 6(d)) was identical to Sensor #3, except that MWCNT thin film #2 was used.

For the final case, Sensor #5 incorporated three sensing

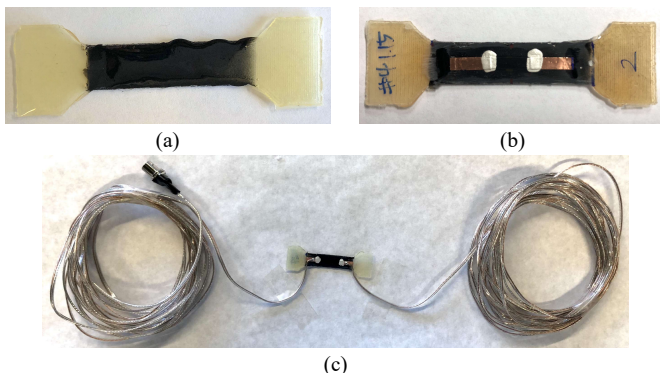

(a)   (b)

(c)

Fig. 4. An MWCNT-based ETDR sensor was assembled by (a) preparing MWCNT-epoxy, (b) attaching MWCNT thin films on it, and (c) connecting the sensing element to the speaker wires.
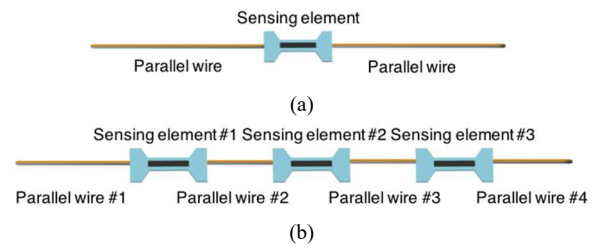

(a)

(b)

Fig. 5. Two different types of MWCNT-based ETDR sensors were used: (a) one sensing element connected to two parallel wires and (b) three sensing elements connected to four parallel wires.

elements for validating distributed strain sensing (Fig. 5(b)), each separated by 4.57 m of parallel wire. It should be noted that the length of the first parallel wire (*i.e.*, between the first sensing element and the BNC connector) was 7.62 m. The sensing elements were identical to those used in Sensor #3, except that the MWCNT-Pluronic films were smaller (3 mm × 11 mm).

E. ETDR strain sensing characterization

All five types of ETDR sensors were subjected to loading-unloading tests. Here, only the MWCNT-based sensing element was mounted in the Test Resources 150R load frame (Fig. 7). A preload of 0.5 N was first applied to ensure that the sensing element was taut. A baseline set of measurements was obtained by using a Keysight 33600A waveform generator to inject a 10 V_{p-p}, 60 MHz, one-cycle, sine wave. A Keysight DSOX3024T digital oscilloscope was also connected to record the reflected waveform response (Fig. 8). Then, a one-cycle uniaxial tensile load pattern to 0.5% was applied to strain the sensing element. The load frame was paused at every 0.1% strain increment to acquire a set of ETDR measurements.

IV. RESULTS AND DISCUSSION

A. Unstrained ETDR sensor response

As discussed in III.E, the ETDR sensors were first mounted in the load frame before they were strained, and baseline ETDR waveforms were obtained. Fig. 9 summarizes the unstrained ETDR measurement results. It can be seen that Sensors #1 to #4 all showed two reflected waves. When an incident wave was transmitted through an ETDR sensor, a portion of the wave reflected (Reflected wave #1) due to impedance mismatch between the sensing element and the parallel wire. The

(a)   (b)
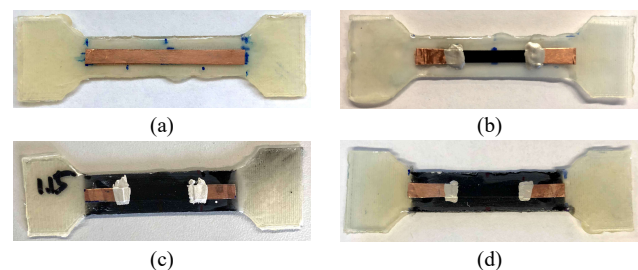
(c)   (d)

Fig. 6. Four types of sensing elements that were fabricated are shown: (a) copper tapes on epoxy; (b) MWCNT thin films on epoxy; (c) MWCNT thin films on MWCNT-epoxy composite; and (d) AC-voltage-treated MWCNT thin films on MWCNT-epoxy composite.
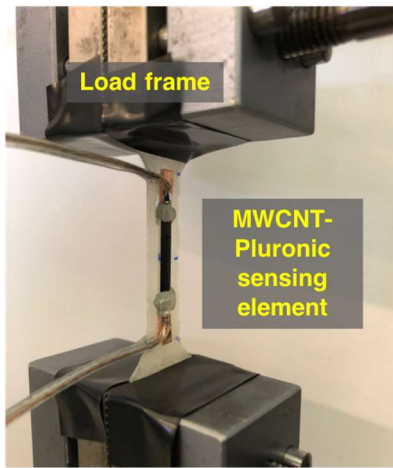
Fig. 7. An MWCNT-based sensing element was mounted in the load frame for strain sensing tests.
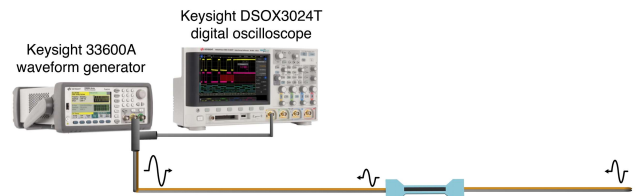

Fig. 8. An ETDR system is composed of a waveform generator, a digital oscilloscope, and the ETDR sensor.

TABLE I
VOLTAGE AMPLITUDES OF REFLECTED WAVES

Sensor ID	Reflected wave #1 voltage [mV]	Reflected wave #2 voltage [mV]
Sensor #1	63	967
Sensor #2	384	517
Sensor #3	363	524
Sensor #4	478	372

remaining portion of the wave was then transmitted, and total reflection occurred (Reflected wave #2) at the end of the ETDR setup due to open-circuit condition ($Z = \infty$). By using (2), the velocity of the transmitted wave was estimated as $v = 2.05 \times 10^8$ m/s, which is ~ 69% the speed of light ($c = 2.99 \times 10^8$ m/s). The time difference (Δt) between the incident wave and Reflected wave #1 was similar among the four sensors ($\Delta t \sim 74$ ns), since the location of each sensing element was identical ($l = 7.62$ m).

On the other hand, the amplitudes of the reflected waves' voltages were different due to impedance differences among the four sensing elements, which are summarized in Table 1. The

voltage amplitude of Reflected wave #1 of Sensor #1 was lower than the other three. This was expected since the resistance of the copper tape ($R = 0.02$ Ω) was much lower than that of the MWCNT-Pluronic thin films in the other sensing elements. Thus, more energy was transmitted through Sensor #1, and total reflection occurred at the end of the sensor so that the amplitude of Reflected wave #2 of Sensor #1 was the highest (Fig. 9(a)).

For both Sensors #2 and #3, MWCNT thin film #1 was used. The difference was that MWCNT-epoxy was used for Sensor #3. This resulted in a smaller reflected voltage amplitude for Sensor #3 (Fig. 9(c)), which can be explained by the sensing
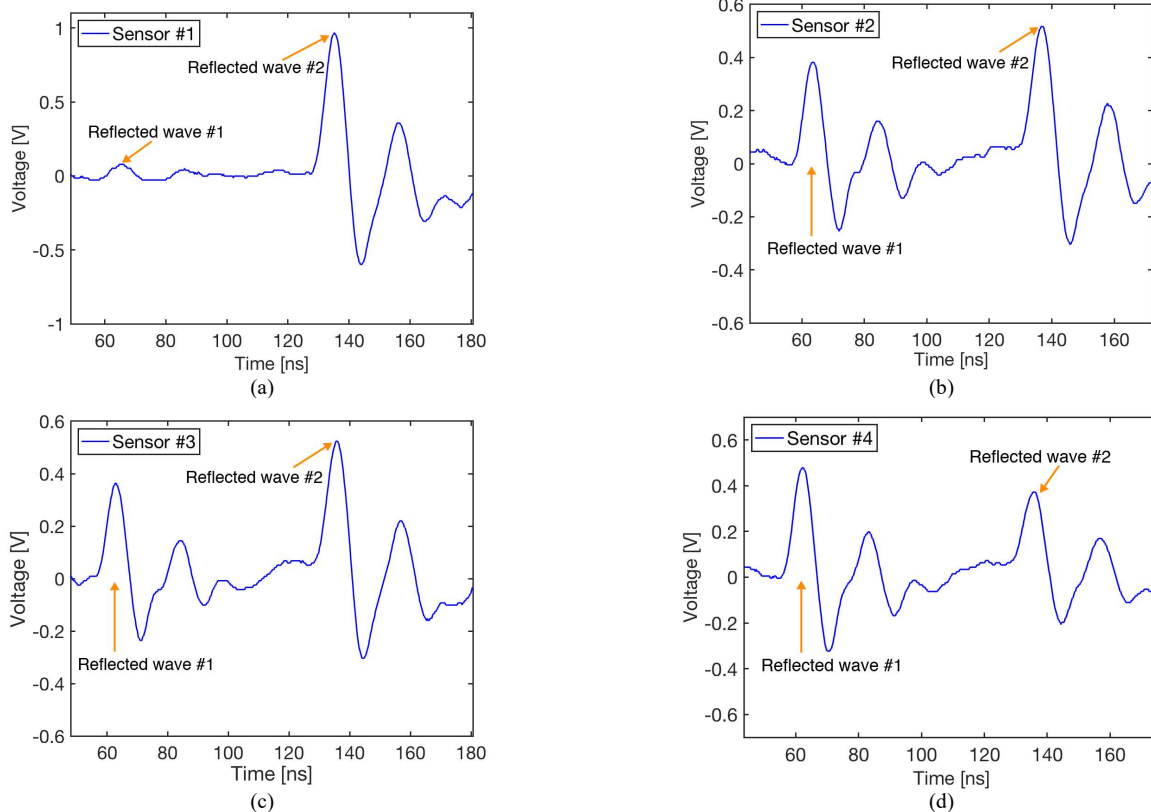

(a)

(b)

(c)

(d)

Fig. 9. The waveform response of each unstrained ETDR sensor is shown: (a) Sensor #1; (b) Sensor #2; (c) Sensor #3; and (d) Sensor #4.

element's C component. It was shown that the dielectric constant of polymer composites was enhanced with the inclusion of CNTs [36, 37], thereby increasing the capacitance and decreasing the impedance.

Although MWCNT-epoxy was used for both Sensors #3 and #4, the voltage amplitude of Reflected wave #1 was higher for Sensor #4 (478 mV) due to its R component. R of Sensor #3 was ~ 42 Ω while that of Sensor #4 was ~ 65 Ω. A possible underlying mechanism is that aligned MWCNTs are less likely to overlap and form connective conducting pathways due to their high length-to-diameter ratio (*i.e.*, aspect ratio). Therefore, given the larger impedance of the conductor in the transmission line, this resulted in a larger reflected wave voltage amplitude for Sensor #4.

B. ETDR strain sensing results

After the baseline ETDR measurements, one cycle of uniaxial tensile strains was applied to each sensing element. Fig. 10 summarizes the response of Sensor #2. Fig. 10(a) overlays the voltage peaks of Reflected wave #1 with respect to different applied strain states. The voltage peak increased as the sensing element was strained in tension. The results can be explained by results from a previous study, where the electrical resistance of MWCNT-based thin films increased when strained in tension [29]. To better quantify strain sensing behavior, the change in voltages (ΔV) with respect to the

unstrained peak voltage was calculated:

$$\Delta V = V_i - V_0 \tag{3}$$

where V_i is the peak voltage of the reflected wave at the ith strain state, and V_0 is the peak voltage of the initial unstrained reflected wave. Fig. 10(b) shows that ΔV changed in tandem with applied stains, thus validating strain sensing using ETDR.

Similar to Sensor #2, ΔV of Sensors #3 (Fig. 11) and #4 (Fig. 12) followed the applied strain pattern as well. To compare the strain sensing behavior among all four sample sets, their ΔV responses were overlaid and shown in Fig. 13. First, Sensor #1 exhibited the worst performance. Sensor #1 used copper tape as conductors, and its electrical impedance did not respond to strain. Second, ΔV of Sensors #2 and #3 were comparable, but Sensor #3 showed slightly higher ΔV at 0.5 % strain ($\Delta V = 76.0$ mV) versus Sensor #2 ($\Delta V = 64.7$ mV). Last, Sensor #4 demonstrated the highest sensitivity to applied strains.

To investigate the underlying mechanism of the results obtained in Fig. 13, the sensitivity of R (for the conductor) and C (for the dielectric) to applied strains were individually analyzed. First, C was investigated by measuring capacitance of epoxy and MWCNT-epoxy as they were strained. When specimens are subjected to deformation, C would be varied, because the thickness, area, and dielectric constant of the
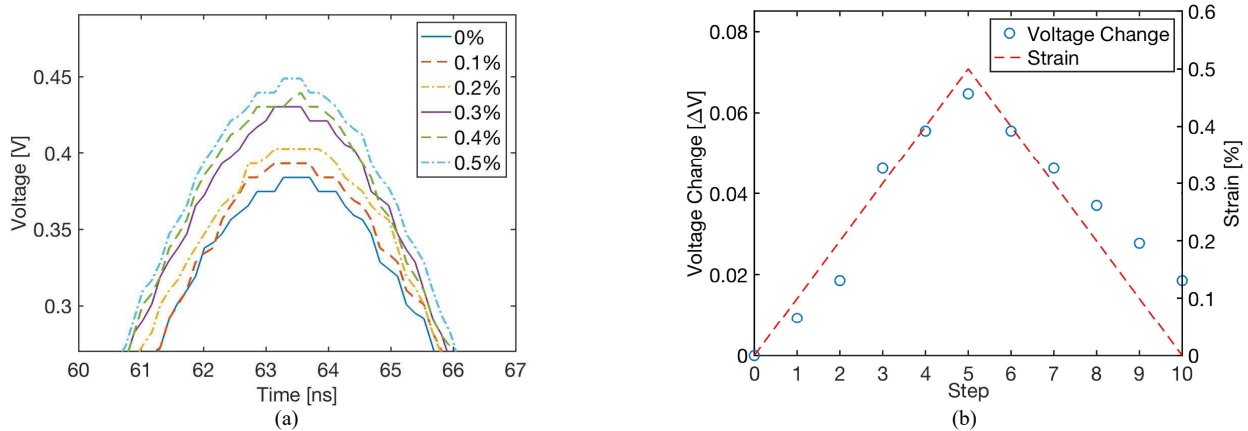

Fig. 10. Sensor #2 was subjected to uniaxial tensile loading and unloading. (a) The peaks of the reflected waves at different strain states are overlaid, and (b) the changes in peak voltage are overlaid with the applied strains.
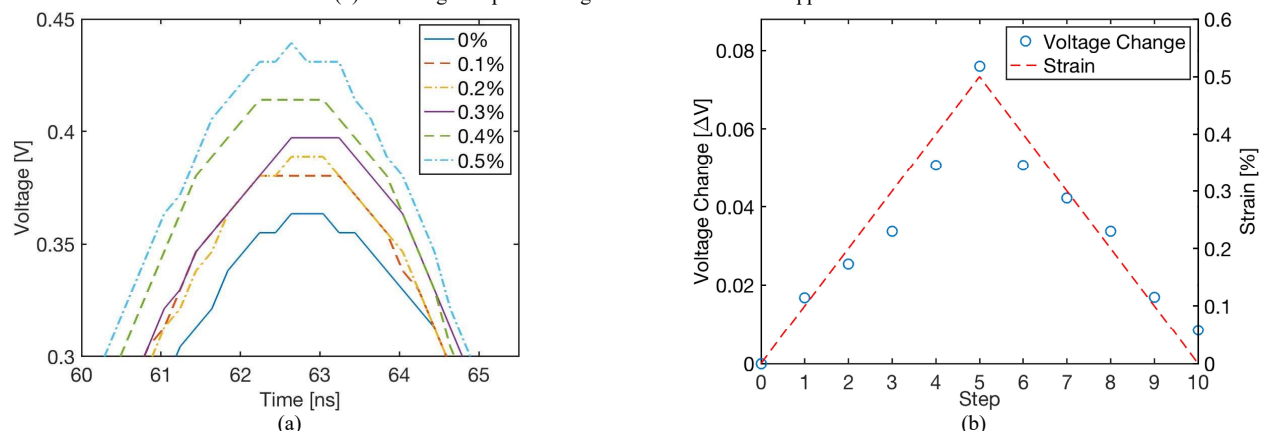

Fig. 11. Sensor #3 was subjected to uniaxial tensile loading and unloading. (a) The peaks of the reflected waves at strain states are overlaid, and (b) the changes in peak voltage are overlaid with the applied strains.
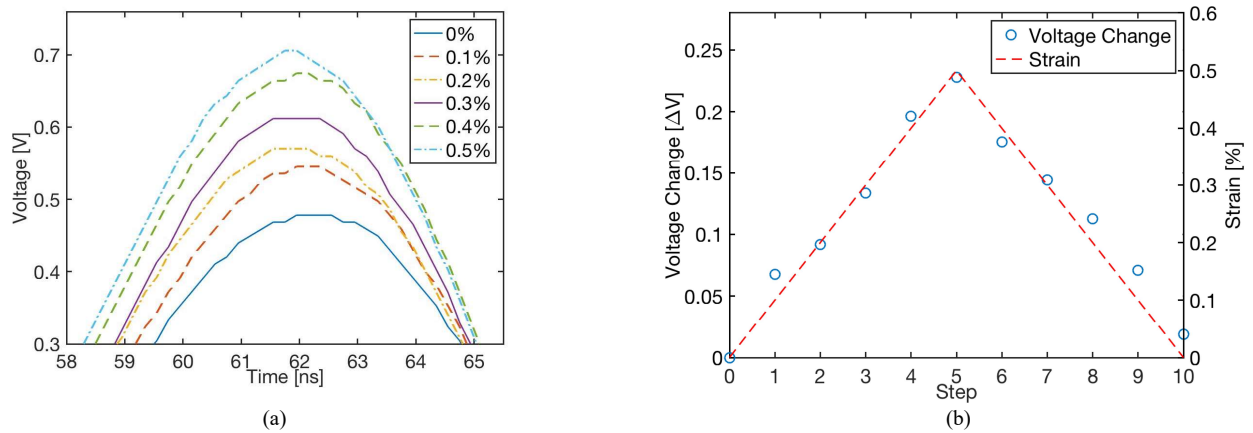
(a)

(b)

Fig. 12. Sensor #4 was subjected to uniaxial tensile loading and unloading. (a) The peaks of the reflected waves corresponding different strain states are overlaid, and (b) the changes in peak voltage and the applied strains are plotted as a function of steps.

specimen changes [38]. Rectangular epoxy films (10 mm × 60 mm × 1 mm) were prepared, and copper films (10 mm × 38 mm) were affixed to its top and bottom surfaces. Similar to the aforementioned ETDR strain sensing tests, the specimen was loaded by applying one cycle of tensile strains and pausing every 0.125% for capacitance measurements using a Keysight E49080A LCR meter. The procedure was repeated until a maximum strain of 0.75% was reached, which was followed by unloading to 0%. The LCR meter applied a 1 V_{p-p}, 2 MHz, sinusoidal excitation signal.

To compare the capacitance results, normalized change in capacitance (C_{norm}) was calculated:

$$C_{norm} = \frac{\Delta C_i}{C_0} \qquad (4)$$

where C_0 is the initial unstrained capacitance of the specimen, and C_i is the change in capacitance at the ith strain state. Representative results of the pristine and MWCNT-epoxy are shown in Fig. 14. It can be seen that C_{norm} of both specimens followed the applied strain pattern, but C_{norm} for the MWCNT-epoxy was more sensitive to applied strains, which is consistent with other studies [18]. Although capacitance was measured at a lower frequency (f = 2 MHz) as compared to the ETDR excitation signal, it was found that the dielectric constant (or capacitance) plateaus at frequencies above 10 kHz [39].
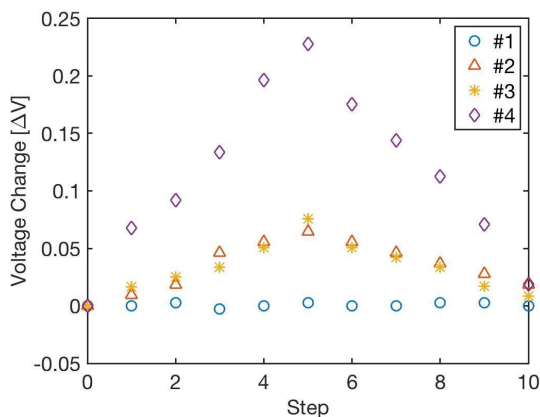
Second, the R component of the ETDR sensing element was

also tested. Here, MWCNT thin films #1 and #2 were prepared. Each thin film was attached to the dog-bone shaped epoxy. The dimensions of the film and gage length between electrodes were consistent with previous ETDR tests. The specimens were mounted in the load frame and subjected to two cycles of tensile loading-unloading at a strain rate of 0.04%/min and to a maximum strain of 0.5%. Fig. 15 summarizes the results. The unstrained resistance of MWCNT thin film #1 ($R = 44.2\,\Omega$) was lower than that of #2 ($R = 63.6\,\Omega$). It can be observed from Figs. 15(a) and 15(c) that both thin films showed linear strain sensing response. Their strain sensitivity or gage factor can be calculated using:
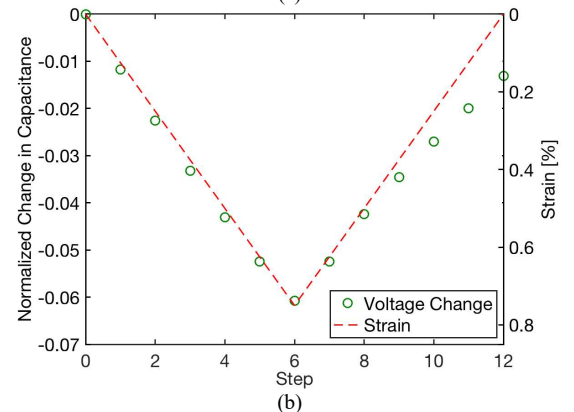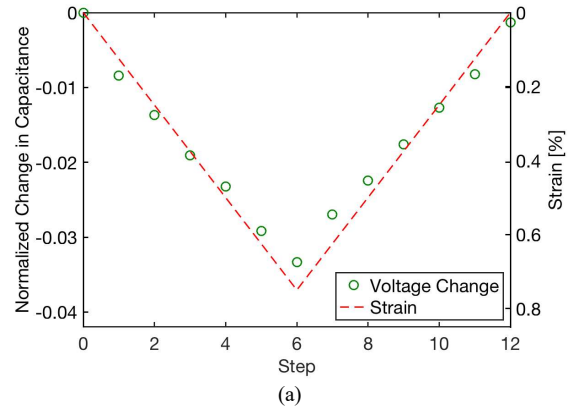

(a)

(b)

Fig. 14. Normalized changes in capacitances overlaid with applied strain patterns are shown: (a) epoxy and (b) MWCNT-epoxy composite.

Fig. 13. The changes in peak voltages of Sensors #1 to #4 are plotted as a function of steps.
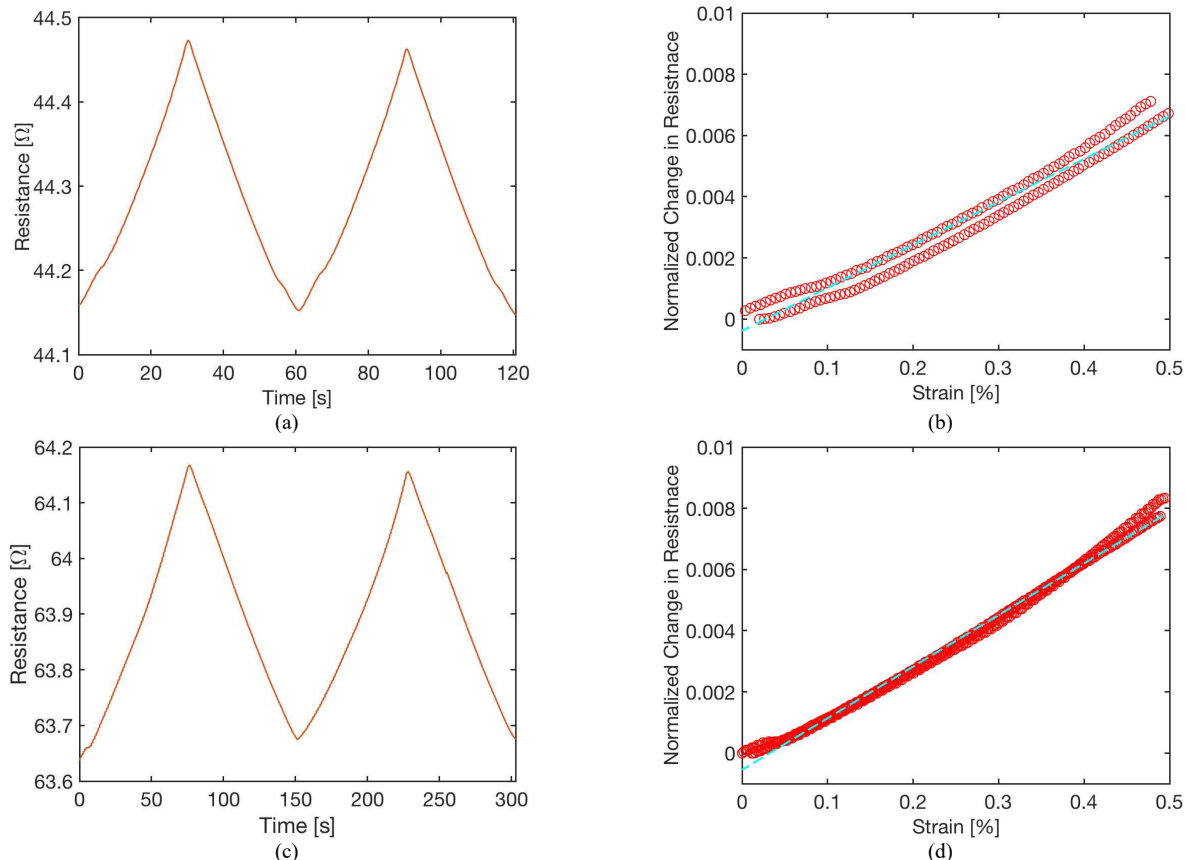
Fig. 15. (a) The electrical resistance response of MWCNT thin film #1 is shown. (b) The normalized change in resistance of MWCNT thin film #1 is plotted as a function of applied strains. (c) The electrical resistance time history of MWCNT thin film #2 is plotted. (d) The normalized change in resistance of MWCNT thin film #2 versus applied strains is shown.

$$S = \frac{R_{norm}}{\Delta\varepsilon} \qquad (5)$$

where R_{norm} is the normalized change in resistance, and $\Delta\varepsilon$ is the corresponding change in applied strain. S for each specimen was estimated by fitting a linear least-squares regression line to the plot of R_{norm} versus strain (Figs. 15(b) and 15(d)). It was found that S for MWCNT thin film #2 ($S = 1.62$) was higher than that of #1 ($S = 1.41$). In fact, when high electric fields are applied to nanocomposites, nanotubes would align along the direction of the field and produce higher bulk strain sensitivity [40]. The increase in strain sensitivity of the thin film directly translated to higher ETDR strain sensitivity. These results suggest that the R component and its piezoresistivity are dominating factors that influence ETDR strain sensing performance. In addition, by manipulating the sensing element's nanostructure, ETDR strain sensing response can be designed or tuned.

C. Distributed strain sensing validation

Finally, distributed strain sensing was validated using Sensor #5 that included three sensing elements in the transmission line. The electrical resistance of all MWCNT thin films was $\sim 20\ \Omega$. As before, a set of baseline ETDR measurements was obtained prior to straining the sensing elements. Fig. 16 shows that the measured response is somewhat complicated. However, the

location of the incident wave ($t = 7.72$ ns), which is not shown in Fig. 16, and that of the final reflected wave (Reflected wave #4) are apparent ($t = 214.60$ ns). Thus, the velocity of the EM wave can be calculated using (2) to give $v = 2.06 \times 10^8$ m/s. With the known location of the three sensing elements, the locations of other reflected waves could be estimated and are marked in Fig. 16.

Strain sensing tests were then performed by straining one of the three sensing elements while keeping the others unstrained. This was repeated until all of the sensing elements were strained and tested. The results are presented in Fig. 17. Similar to Sensors #2 to #4 with one sensing element, all the Sensing
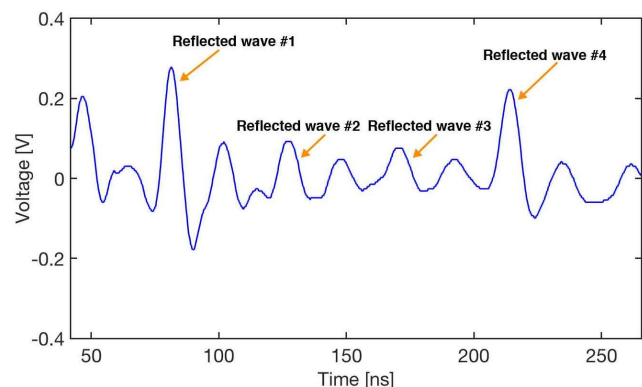

Fig. 16. The waveform response of Sensor #5 is plotted as a function of time.
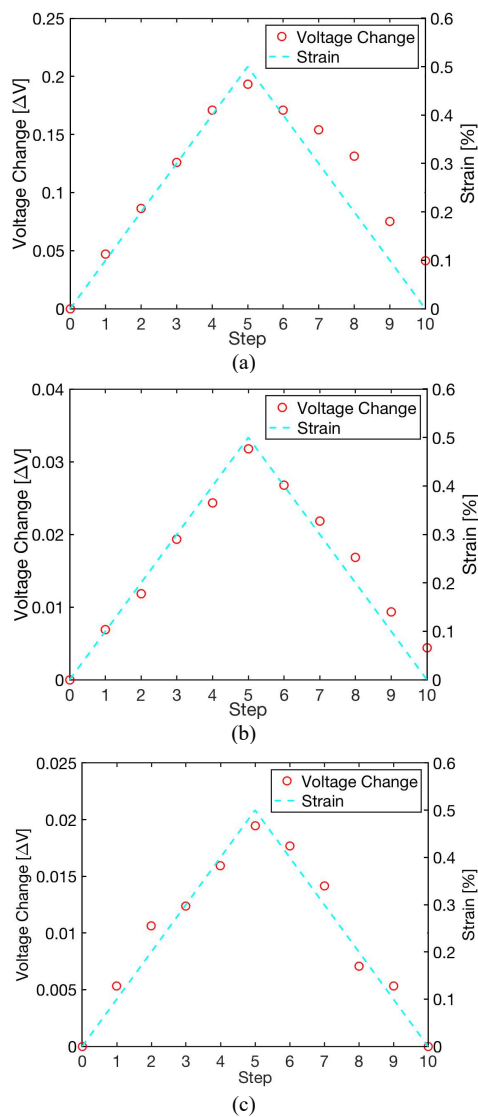
Fig. 17. Each sensing element of Sensor #5 was subjected to strain sensing tests. (a) The changes in peak voltage of Sensing element #1, (b) Sensing element #2, and (c) Sensing element #3 are overlaid with the (same) applied strain pattern.

elements #1 to #3 clearly showed strain sensing behavior, where their voltage change matched the applied strain pattern, thereby successfully validating distributed sensing. However, the voltage change degraded as the location of sensing element was farther from the probe. To be specific, the first sensing element exhibited greater voltage changes than the other two. A possible explanation can be due to signal attenuation that worsened as the EM wave traveled down the transmission line and with a portion of the energy of the wave lost due to reflections as it interacted with each additional sensing element.

V. CONCLUSIONS

In this study, a new approach for truly distributed strain sensing was demonstrated by integrating ETDR with MWCNT-based sensing elements. This work investigated different types of sensing elements, where the conductor was formed using MWCNT-Pluronic thin films, and the dielectric was either

pristine or MWCNT-epoxy thick films. Upon integration of these sensing elements in a transmission line, the results showed that all the ETDR responses showed voltage changes that varied linearly with respect to applied strains. Furthermore, it was found that the strain sensitivity or gage factor of the MWCNT-Pluronic thin film conductor element directly influenced the bulk strain sensitivity of the ETDR sensor. The results suggested that the desired strain sensing performance of ETDR sensors could be achieved by controlling thin film nanostructure. Last, to validate distributed strain sensing, three sensing elements were integrated in a single transmission line. Each sensing element was subjected to applied strains, while their voltage responses were recorded using ETDR. Strain sensitivity was confirmed for all the sensing elements, and ETDR could successfully interrogate and acquire their response simply by analyzing the recorded reflected voltage waveforms. The achievable spatial resolution of the distributed sensor was primarily controlled, of course, by the speed of the EM pulse on the sensing line. Further control on spatial resolution can be achieved by tailoring the excitation pulse. Future work will build on these preliminary results to improve the strain sensitivity and optimize the achievable spatial resolution by excitation pulse tailoring.

REFERENCES

[1] C. R. Farrar, and K. Worden, "An introduction to structural health monitoring," *Philos. Trans. A Math. Phys. Eng. Sci.,* vol. 365, no. 1851, pp. 303-315, 2007.

[2] S. R. Hunt, and I. G. Hebden, "Validation of the Eurofighter Typhoon structural health and usage monitoring system," *Smart Mater. Struct.,* vol. 10, no. 3, pp. 497-503, 2001.

[3] S. J. Mihailov, "Fiber Bragg grating sensors for harsh environments," *Sensors,* vol. 12, no. 2, pp. 1898-1918, 2012.

[4] X. Bao, and L. Chen, "Recent progress in distributed fiber optic sensors," *Sensors,* vol. 12, no. 7, pp. 8601–8639, June, 2012.

[5] R. Di Sante, "Fibre optic sensors for structural health monitoring of aircraft composite structures: recent advances and applications," *Sensors,* vol. 15, no. 8, pp. 18666-18713, July, 2015.

[6] M. K. Barnoski, M. D. Rourke, S. M. Jensen, and R. T. Melville, "Optical time domain reflectometer," *Appl. Opt.,* vol. 16, no. 9, pp. 2375-2379, September, 1977.

[7] J. C. Juarez, and H. F. Taylor, "Polarization discrimination in a phase-sensitive optical time-domain reflectometer intrusion-sensor system," *Opt. Lett.,* vol. 30, no. 24, pp. 3284-3286, December, 2005.

[8] C. H. Dowding, M. B. Su, and K. O'Connor, "Measurement of rock mass deformation with grouted coaxial antenna cables," *Rock Mech. Rock Eng.,* vol. 22, no. 1, pp. 1-23, January, 1989.

[9] K. Noborio, "Measurement of soil water content and electrical conductivity by time domain reflectometry: a review," *Comput. Electron. Agric.,* vol. 31, no. 3, pp. 213-237, May, 2001.

[10] W. Liu, R. G. Hunsperger, M. J. Chajes, K. J. Folliard, and E. Kunz, "Corrosion Detection of Steel Cables using Time Domain Reflectometry," *J. Mater. Civ. Eng.,* vol. 14, no. 3, pp. 217-223, 2002.

[11] M. W. Lin, J. Thaduri, and A. O. Abatan, "Development of an electrical time domain reflectometry (ETDR) distributed strain sensor," *Meas. Sci. Technol.,* vol. 16, no. 7, pp. 1495–1505, 2005.

[12] D. M. Pozar, *Microwave engineering*, 4th ed., NJ: Wiley, 2012.

[13] M. W. Lin, A. O. Abatan, and W.-M. Zhang, "Crack damage detection of concrete structures using distributed electrical time domain reflectometry (ETDR) sensors," in 1999 Symposium on Smart Structures and Materials. pp. 297-304.

[14] D. Panth, "Reasons for failure of transmission lines and their prevention strategies," *IJEEDC,* vol. 2, no. 1, pp. 1-4, 2014.

[15] G. D. Chen, S. S. Sun, D. Pommerenke, J. L. Drewniak, G. G. Greene, R. D. McDaniel, A. Belarbi, and H. M. Mu, "Crack detection of a full-scale reinforced concrete girder with a distributed cable sensor," *Smart Mater. Struct.,* vol. 14, no. 3, pp. S88–S97, 2005.

[16] A. Todoroki, K. Ohara, Y. Mizutani, Y. Suzuki, and R. Matsuzaki, "Self-sensing time-domain reflectometry for detection of the bearing failure of a CFRP laminate fastener hole: effect of peeling of the insulator," *Adv. Compos. Mater,* vol. 25, no. 5, pp. 457-469, September, 2016.

[17] G. Pandey, M. Wolters, E. T. Thostenson, and D. Heider, "Localized functionally modified glass fibers with carbon nanotube networks for crack sensing in composites using time domain reflectometry," *Carbon,* vol. 50, no. 10, pp. 3816-3825, August, 2012.

[18] A. Sanli, C. Müller, O. Kanoun, C. Elibol, and M. F. X. Wagner, "Piezoresistive characterization of multi-walled carbon nanotube-epoxy based flexible strain sensitive films by impedance spectroscopy," *Compos. Sci. Technol.,* vol. 122, pp. 18-26, January, 2016.

[19] G. Esen, M. S. Fuhrer, M. Ishigami, and E. D. Williams, "Transmission line impedance of carbon nanotube thin films for chemical sensing," *Appl. Phys. Lett.,* vol. 90, no. 12, pp. 123510, 2007.

[20] T. N. Tallman, S. Gungor, K. W. Wang, and C. E. Bakis, "Damage detection via electrical impedance tomography in glass fiber/epoxy laminates with carbon black filler," *Structural Health Monitoring,* vol. 14, no. 1, pp. 100-109, 2015.

[21] R. Jan, A. Habib, Z. M. Khan, M. B. Khan, M. Anas, A. Nasir, and S. Nauman, "Liquid exfoliated graphene smart layer for structural health monitoring of composites," *J. Intell. Mater. Syst. Struct.,* vol. 28, no. 12, pp. 1565-1574, 2017.

[22] L. M. Chiacchiarelli, M. Rallini, M. Monti, D. Puglia, J. M. Kenny, and L. Torre, "The role of irreversible and reversible phenomena in the piezoresistive behavior of graphene epoxy nanocomposites applied to structural health monitoring," *Compos. Sci. Technol.,* vol. 80, pp. 73-79, May, 2013.

[23] L. Vertuccio, L. Guadagno, G. Spinelli, P. Lamberti, V. Tucci, and S. Russo, "Piezoresistive properties of resin reinforced with carbon nanotubes for health-monitoring of aircraft primary structures," *Composites Part B,* vol. 107, pp. 192-202, December, 2016.

[24] J. Sebastian, N. Schehl, M. Bouchard, M. Boehle, L. Li, A. Lagounov, and K. Lafdi, "Health monitoring of structural composites with embedded carbon nanotube coated glass fiber sensors," *Carbon,* vol. 66, pp. 191-200, January, 2014.

[25] S. Sun, B. Han, S. Jiang, X. Yu, Y. Wang, H. Li, and J. Ou, "Nano graphite platelets-enabled piezoresistive cementitious composites for structural health monitoring," *Construct. Build. Mater.,* vol. 136, pp. 314-328, April, 2017.

[26] Y. Zhang, N. Anderson, S. Bland, S. Nutt, G. Jursich, and S. Joshi, "All-printed strain sensors: Building blocks of the aircraft structural health monitoring system," *Sens. Actuators A,* vol. 253, pp. 165-172, January, 2017.

[27] S.-H. Hwang, H. W. Park, and Y.-B. Park, "Piezoresistive behavior and multi-directional strain sensing ability of carbon nanotube–graphene nanoplatelet hybrid sheets," *Smart Mater. Struct.,* vol. 22, no. 1, 2013.

[28] M. Amjadi, K. U. Kyung, I. Park, and M. Sitti, "Stretchable, skin-mountable, and wearable strain sensors and their potential applications: a review," *Adv. Funct. Mater.,* vol. 26, no. 11, pp. 1678-1698, February, 2016.

[29] B. M. Lee, and K. J. Loh, "Carbon nanotube thin film strain sensors: comparison between experimental tests and numerical simulations," *Nanotechnology,* vol. 28, no. 15, pp. 1-14, 2017.

[30] M. R. Alenezi, S. J. Henley, N. G. Emerson, and S. R. P. Silva, "From 1D and 2D ZnO nanostructures to 3D hierarchical structures with enhanced gas sensing properties," *Nanoscale,* vol. 6, no. 1, pp. 235-247, October, 2014.

[31] J. F. Christ, N. Aliheidari, A. Ameli, and P. Pötschke, "3D printed highly elastic strain sensors of multiwalled carbon nanotube/thermoplastic polyurethane nanocomposites," *Materials & Design,* vol. 131, pp. 394-401, October, 2017.

[32] Y. Yan, V. Sencadas, J. Zhang, G. Zu, D. Wei, and Z. Jiang, "Processing, characterisation and electromechanical behaviour of elastomeric multiwall carbon nanotubes-poly (glycerol sebacate) nanocomposites for piezoresistive sensors applications," *Compos. Sci. Technol.,* vol. 142, pp. 163-170, April, 2017.

[33] B. R. Loyola, Y. Zhao, K. J. Loh, and V. L. Saponara, "The electrical response of carbon nanotube-based thin film sensors subjected to mechanical and environmental effects," *Smart Mater. Struct.,* vol. 22, no. 2, pp. 1-11, December, 2013.

[34] J. Kim, K. J. Loh, and J. P. Lynch, "Piezoelectric polymeric thin films tuned by carbon nanotube fillers," in SPIE – 15th Annual International Symposium on Smart Structures and Materials.

[35] A. I. Oliva-Avilés, F. Avilés, V. Sosa, A. I. Oliva, and F. Gamboa, "Dynamics of carbon nanotube alignment by electric fields," *Nanotechnology,* vol. 23, no. 46, 2012.

[36] C. Yang, Y. Lin, and C. W. Nan, "Modified carbon nanotube composites with high dielectric constant, low dielectric loss and large energy density," *Carbon,* vol. 47, no. 4, pp. 1096-1101, April, 2009.

[37] L. Wang, and Z.-M. Dang, "Carbon nanotube composites with high dielectric constant at low percolation threshold," *Appl. Phys. Lett.,* vol. 87, no. 4, 2005.

[38] H. Y. Lee, and Y. M. Shkel, "Dielectric response of solids for contactless detection of stresses and strains," *Sens. Actuators A,* vol. 137, no. 2, pp. 287-295, July, 2007.

[39] X. Guo, D. Yu, Y. Gao, Q. Li, W. Wan, and Z. Gao, "Dielectric properties of filled carbon nanotubes/epoxy composites with high dielectric constant," in 2006 1st IEEE International Conference on Nano/Micro Engineered and Molecular Systems. pp. 295-298.

[40] A. I. Oliva-Avilés, F. Avilés, and V. Sosa, "Electrical and piezoresistive properties of multi-walled carbon nanotube/polymer composite films aligned by an electric field," *Carbon,* vol. 49, no. 9, pp. 2989-2997, August, 2011.

Bo Mi Lee was born in Anyang, South Korea, in 1986. She received the B.S. degree in physics from Hanyang University, Ansan, South Korea, in 2009. She received the M.S. degree in civil and environmental engineering from Korea Advanced Institute and Technology (KAIST), Daejeon, South Korea, in 2011. She is currently a Ph.D. candidate in structural engineering in University of California-San Diego, La Jolla, CA, USA. She is a member of the Active, Responsive, Multifunctional, and Ordered-materials Research (ARMOR) Laboratory. Her research interests include multiscale modeling, multifunctional materials, structural health monitoring, and energy harvesting.
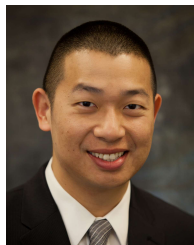
Kenneth J. Loh (Member, IEEE) was born in Urbana, IL, USA, in 1982. He received the B.S. degree in civil engineering from Johns Hopkins University, Baltimore, MD, USA, in 2004. Thereafter, he received the M.S. degrees in civil engineering (2005) and in materials science and engineering (2008), as well as the Ph.D. degree in civil engineering (2008), all from the University of Michigan, Ann Arbor, MI, USA.

He is currently a Professor in the Structural Engineering Department at the University of California-San Diego, La Jolla, CA, USA. He is also the director of the ARMOR Lab and the associate director for the Center of Extreme Events Research (CEER) at the University of California-San Diego. Prior to this, he was an Assistant and then Associate Professor with the Civil and Environmental Engineering Department at the University of California-Davis, CA, USA, from 2008 to 2015. Prof. Loh is a Senior Member of SPIE, and his recent awards include: the 2018 Structural Health Monitoring Person-of-the-Year Award;

2014 Outstanding Junior Faculty Award at UC Davis; 2013 NSF CAREER award; and the 2013 Achenbach Medal. His research interests include multifunctional materials, stimuli-responsive nanocomposites, and tomographic methods for applications in human health/performance assessment and structural health monitoring.

Francesco Lanza di Scalea (Senior Member, IEEE) was born in Palermo, Italy, in 1969. He received the Laurea (*summa cumlaude*) and Ph.D. degrees in mechanical engineering from the University of Palermo, Palermo, in 1993 and 1997, respectively. As a Fulbright Student, he also received the M.S. degree in Engineering Mechanics from Michigan State University, East Lansing, MI, USA, in 1996. From 1998 to 1999, he was a Post-Doctoral Fellow with the Center for Nondestructive Evaluation, Materials Science and Engineering Department, of the Johns Hopkins University, Baltimore, MD, USA.

Since 1999, he has been a Faculty Member with the Department of Structural Engineering, University of California in San Diego, La Jolla, CA, USA, where he is currently a Full Professor and the Director of the NDE & Structural Health Monitoring Laboratory. His current research and teaching interests include nondestructive evaluation, structural health monitoring, experimental mechanics, smart structures, and digital signal processing.

Prof. Lanza di Scalea was elected Fellow of the Acoustical Society of America (ASA), of the Society for Experimental Mechanics (SEM), and of the American Society for Nondestructive Testing (ASNT). He is a Senior Member of IEEE. He was awarded the UCSD Structural Engineering Department's Best Teacher Award in 2011, the Structural Health Monitoring Person-of-the-Year Award in 2007, the American Society for Nondestructive Testing Research Fellowship Award in 2002, 2006, and 2010, the American Society for Nondestructive Testing Faculty Grant Award in 2003, the UCSD Hellman Faculty Fellowship in 2000 and 2002, and the U.S. Institute for International Education Fulbright Scholarship in 1995. He is a member of the Railway Maintenance Committee (AR060) of the U.S. Transportation Research Board. He currently serves on the Editorial Boards of the *Journal of Intelligent Materials Systems and Structures*, *Experimental Mechanics*, *Research in Nondestructive Evaluation*, and *Structural Health Monitoring: An International Journal*.